



HAL
open science

Transverse Mixing in Rivers With Longitudinally Varied Morphology

Lorris Gond, Emmanuel Mignot, J. Le Coz, L. Kateb

► **To cite this version:**

Lorris Gond, Emmanuel Mignot, J. Le Coz, L. Kateb. Transverse Mixing in Rivers With Longitudinally Varied Morphology. *Water Resources Research*, 2021, 57 (6), pp.e2020WR029478. 10.1029/2020wr029478 . hal-03515534

HAL Id: hal-03515534

<https://hal.inrae.fr/hal-03515534>

Submitted on 6 Jan 2022

HAL is a multi-disciplinary open access archive for the deposit and dissemination of scientific research documents, whether they are published or not. The documents may come from teaching and research institutions in France or abroad, or from public or private research centers.

L'archive ouverte pluridisciplinaire **HAL**, est destinée au dépôt et à la diffusion de documents scientifiques de niveau recherche, publiés ou non, émanant des établissements d'enseignement et de recherche français ou étrangers, des laboratoires publics ou privés.

Water Resources Research

RESEARCH ARTICLE

10.1029/2020WR029478

Key Points:

- Tracing experiments in a shallow, gravel-bedded river yield highly variable transverse mixing coefficients
- Usual predictive formulas fail to predict reach-averaged transverse mixing coefficients in a river with longitudinally varied morphology
- An equation based on a flow nonuniformity parameter is fitted to our experimental data

Correspondence to:

L. Gond,
lorris.gond@insa-lyon.fr

Citation:

Gond, L., Mignot, E., Le Coz, J., & Kateb, L. (2021). Transverse mixing in rivers with longitudinally varied morphology. *Water Resources Research*, 57, e2020WR029478. <https://doi.org/10.1029/2020WR029478>

Received 19 JAN 2021

Accepted 1 MAY 2021

Transverse Mixing in Rivers With Longitudinally Varied Morphology

L. Gond^{1,2,3} , E. Mignot¹, J. Le Coz², and L. Kateb³

¹University Lyon, INSA Lyon, Ecole Centrale de Lyon, CNRS, LMFA, Villeurbanne, France, ²INRAE Lyon-Grenoble, UR Riverly, Villeurbanne, France, ³CEA, DES, IRESNE, DTN, Laboratoire de Modélisation des Transferts dans l'Environnement, Saint-Paul-Lez-Durance, France

Abstract Improving the quantification of the transverse mixing coefficient in rivers is essential for a better estimation of pollutant dispersion. This coefficient is evaluated from tracing experiments or from semi-empirical equations assuming uniform flow conditions. This assumption, verified for laboratory experiments, is questionable for river studies. For example, piedmont rivers exhibit nonuniform flows due to their longitudinal morphological variations. This work aims at studying the longitudinal variability of the transverse mixing coefficient in a river with longitudinally varied morphology and the overlooked impact of the flow nonuniformity on the coefficient's values. Tracing experiments were conducted in the Durance River in France using slug injections and concentration measurements made at the cross-sections delineating homogeneous sub-reaches. Using the well-known 1D transverse diffusion model, values of the transverse mixing coefficient are determined for all consecutive sub-reaches. These values substantially vary along the studied river, with stronger mixing efficiency at pools and complex riffles and weaker mixing efficiency in straight sub-reaches with emerging obstacles. The dimensionless transverse mixing coefficient is strongly related to a parameter quantifying the deviation from flow-uniformity, i.e., indicating flow acceleration, deceleration or a succession of both within the sub-reaches. While usual formulas from the literature fail to predict our empirical results, a new equation including the flow nonuniformity parameter fits our experimental data with high accuracy. After further validation, such equation may be used for predicting the transverse mixing coefficient in rivers with longitudinally varied morphology.

1. Introduction

Predicting the spatial distribution of pollutant concentration in rivers downstream from point sources, e.g., industrial or urban water waste releases or accidental spillings, is critical for assessing water quality and aquatic wildlife sustainability. At large scale, a pollutant in a river mostly spreads in the longitudinal direction, but more locally and closer to the source, spreading also takes place in the transverse direction, until a uniform concentration is reached across the river width (Rutherford, 1994). 1D or 2D numerical modeling of pollutant dynamics (Abderrezzak et al., 2015; Seo et al., 2016) then requires values of both longitudinal and transverse mixing coefficients.

The transverse mixing coefficient E_y (m^2/s) is a catch-all coefficient lumping the contributions of different processes to the transverse mixing: molecular diffusion, usually negligible, turbulent diffusion, and dispersion due to secondary circulations (Rutherford, 1994; Yotsukura & Sayre, 1976). Many experiments in laboratory flumes (Elder, 1959; Fischer, 1969; Okoye, 1970; Webel & Schatzmann, 1984) and in rivers (Demetropoulos & Stefan, 1983; Fischer, 1973; Sayre & Yeh, 1973; Seo et al., 2006, 2016; Yotsukura & Cobb, 1972) were performed in order to evaluate the transverse mixing coefficient under different flow conditions, by injecting a substance in a stream, measuring concentration cross-profiles further downstream, and calibrating a 1D transverse diffusion model (Rutherford, 1994) based on the measurements. These experiments enabled various authors (e.g., Aghababaei et al., 2017; Deng et al., 2001; Huai et al., 2018; Jeon et al., 2007) to analyze the influence of the reach-scale geometric and hydraulic parameters on the transverse mixing coefficient and proposed empirical equations predicting the coefficient. These equations are usually based on a function φ of three dimensionless parameters derived from the dimensional analysis, in the form:

$$\frac{E_y}{LV} = \varphi \left(\frac{U}{u_*}, \frac{W}{H}, S_n \right) \quad (1)$$

where L is a characteristic length, generally taken equal to the reach-averaged flow depth H (m) or width W (m), V is a characteristic velocity, taken equal to the reach-averaged velocity $U = Q / (WH)$ (m/s) with Q the flow discharge (m³/s), or to the shear velocity u_* (m/s). The parameter S_n is the channel sinuosity (the ratio between the curvilinear length and the Euclidean distance between two points of the flow axis), sometimes replaced by H / R_c (Fischer, 1969) or W / R_c (Yotsukura & Sayre, 1976) with R_c the curvature radius of the channel in the case of a single bend. Along with the aspect ratio W / H , the sinuosity reflects the mixing due to dispersion by secondary currents in curved channels (Aghababaei et al., 2017; Huai et al., 2018; Jeon et al., 2007), while the so-called friction ratio U / u_* , sometimes replaced by the friction coefficient $\lambda = 8(U / u_*)^2$, reflects the mixing due to turbulent diffusion (Webel & Schatzmann, 1984).

Most predictive equations in the literature are expressed with $L = H$ and $V = u_*$. However, it is not obvious that the same characteristic velocity and length apply to all mixing processes. For instance, Huai et al. (2018) consider $L = H$ for the turbulent diffusion coefficient and $L = W$ for the dispersion coefficient, with $V = u_*$ in both cases. Still, the classification proposed by Rutherford (1994) remains the simplest and most widely used reference to estimate the mixing coefficient in a given river: $E_y / (Hu_*) = 0.15 - 0.3$ for straight channels, $E_y / (Hu_*) = 0.3 - 0.9$ for gently meandering channels, and $E_y / (Hu_*) = 1 - 3$ for sharply curved channels. In straight laboratory flumes, the transverse dimensionless coefficient tends toward a constant value ($E_y / (Hu_*) \approx 0.13$) for high friction coefficients ($\lambda > 0.08$) (Webel & Schatzmann, 1984). This value is consistent with the lower bound for straight channels ($E_y / (Hu_*) = 0.15$) of Rutherford's classification. Nevertheless, for a similar range of hydraulic parameters, values reported from rivers studies can be much higher (see tables in Huai et al., 2018). As a consequence, separate predictive equations are proposed in the literature for rivers and laboratory flumes. It appears that none of the equations dedicated to rivers are able to predict the coefficient values measured in straight channels ($S_n = 1$) in laboratory conditions. Moreover, these equations are unable to predict the highest mixing coefficient values reported in rivers (see Figure 5 of Huai et al., 2018). This suggests that a parameter characterizing an additional mixing process is missing in Equation 1, and that such additional process cannot be represented using a combination of the usual dimensionless parameters: W / H , U / u_* or λ , and S_n or W / R_c .

The values of the transverse mixing coefficient available in the river literature are reach-averaged, i.e., they are estimated from the best-fitting of a 1D diffusion model over relatively long river sections (e.g., few hundred meters to few kilometers). This model considers a uniform flow, i.e., the hydraulic and geometric parameters do not vary substantially along the longitudinal direction between the injection and the measuring cross-sections. This approach leads to accurate values of the mixing coefficient for laboratory experiments and artificial canals (Fischer, 1973) in conditions that meet the 1D model assumptions, but is expected to be less accurate in rivers where hydraulic and geometric parameters are hardly uniform longitudinally, at least over distances of several width long. For example, Figures 9 and 10 of Seo et al. (2006) suggest that the transverse mixing coefficient varies longitudinally within their studied reaches, with successions of stronger and weaker mixing efficiency in between successive measuring cross-sections. Since the predictive equations in rivers (in the form of Equation 1) are constructed from values of reach-averaged transverse mixing coefficient and reach-averaged hydraulic parameters for which the longitudinal flow variations and flow nonuniformity are neglected in the literature, the equations cannot reflect their possible contribution to the transverse mixing.

We assume that the overlooked flow nonuniformity along the river reach may be the reason why existing equations often underestimate the high transverse mixing coefficient values observed in rivers and why they cannot cover both laboratory and field conditions. We suspect that a unified equation for the transverse mixing coefficient should include an additional term quantifying the effect of the flow nonuniformity within the studied area.

This study reports experimental evidence of the longitudinal variability of the transverse mixing coefficient in a short river reach due to flow nonuniformity and proposes an original predictive equation that includes

such effect. The manuscript is organized as follows. Section 2 introduces the theoretical basis for the estimation of the transverse mixing coefficient, including the 1D diffusion model and the spatial averaging of the hydraulic and geometric parameters. Section 3 describes the fieldwork and setup of tracing experiments conducted in consecutive sub-reaches of a 2 km-long reach of the Durance River in France, a shallow gravel-bedded piedmont river. In Section 4, the values of the transverse mixing coefficient within each sub-reach are quantified and discussed with regards to the geometric and hydraulic characteristics of the river sub-reach. A new predictive equation for the nondimensional transverse mixing coefficient is established, including a term for the flow nonuniformity. The findings are discussed in Section 5.

2. Theoretical Considerations

2.1. Diffusion Model Equation

The evaluation of the transverse mixing coefficient in the general case of a reach with longitudinally varied morphology, hence nonuniform flow, leads to a complicated resolution of the advection-diffusion equation, with no analytic solution. The approach followed herein is based on the analytical solution of the advection-diffusion equation for a uniform flow, commonly used in the literature. The effect of flow nonuniformity will be encompassed in the catch-all reach-averaged transverse mixing coefficient as an additional contribution to that of molecular and turbulent diffusion, and dispersion by secondary currents.

As proposed by Beltaos (1975) and Seo et al. (2006) among others, the transverse mixing coefficient in a stream with large aspect ratio can be quantified by applying the streamtube formulation (Yotsukura & Cobb, 1972) of the depth-averaged advection-diffusion equation. This formulation of the advection-diffusion equation introduces a change of coordinates where the 2D cartesian system (x, y) , with x (m) a longitudinal coordinate and y (m) a transverse coordinate, is transformed into a new system (x, q) , where $q = \int_0^y u(s)h(s)ds$ (m^3/s) is the cumulative discharge, with u the local time- and depth-averaged streamwise velocity and h the local water depth.

Compared to constant-rate tracer injections, slug injections, i.e., sudden releases of a mass of tracer, substantially decrease the duration of field experiments and the mass of tracer released into the river (Beltaos, 1975; Seo et al., 2006). The 1D advection-diffusion equation is then solved under the uniformity hypothesis for the depth-averaged dosage $\theta(x, q) = \int_0^\infty C(x, q, t)dt$ ($\text{kg}\cdot\text{s}/\text{m}^3$), where $C(x, q, t)$ is the depth-averaged time-dependent concentration:

$$\frac{\partial \theta}{\partial x} = B \frac{\partial^2 \theta}{\partial q^2} \quad (2)$$

where B is the reach-averaged diffusion factor (m^5/s^2):

$$B = \frac{1}{Q} \int_0^Q u h^2 \varepsilon_y dq = \Psi U H^2 E_y \quad (3)$$

where $\Psi = \frac{1}{Q U H^2} \int_0^Q u(q)h(q)^2 dq$ is the velocity shape factor quantifying the transverse nonuniformity of water depth and streamwise velocity, ε_y (m^2/s) is the local depth-averaged transverse mixing coefficient and $E_y = B / (\Psi H U^2)$ (m^2/s) is the reach-averaged transverse mixing coefficient. Equation 2 can be made dimensionless:

$$\frac{\partial D}{\partial x} = \frac{B}{Q^2} \frac{\partial^2 D}{\partial \eta^2} \quad (4)$$

where $D = \theta / \bar{\theta}$ is the dimensionless local dosage, $\bar{\theta} = M / Q$ is the transverse-averaged dosage, M (kg) the injected mass of tracer, and $\eta = q / Q$ is the dimensionless cumulative discharge.

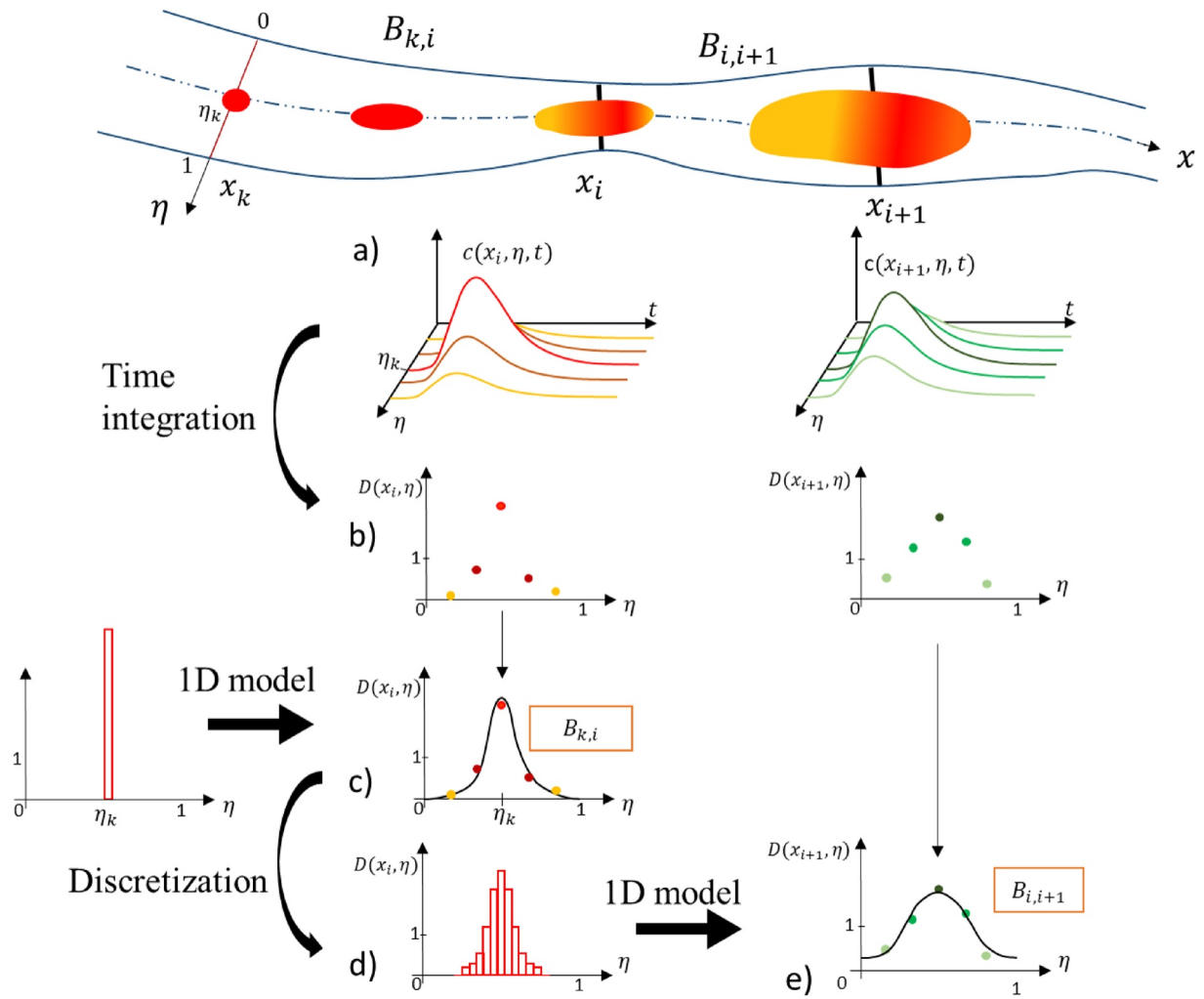


Figure 1. Procedure applied to estimate the transverse mixing coefficients from a slug injection of tracer: (a) concentration measurements at x_i and x_{i+1} , (b) dosage cross-profile calculation at x_i and x_{i+1} , (c) fit of Equation 5 against the concentration profile measured at x_i , (d) discretization of the fitted dosage cross-profile at x_i , (e) fit of Equation 6 against the concentration profile measured at x_{i+1} .

Moreover, as rivers are laterally confined, a specific treatment of the banks is required. The mirror method (Rutherford, 1994) assumes that the dosage is fully reflected by the banks under the Neumann boundary condition: $\partial D / \partial \eta |_{\eta=0} = \partial D / \partial \eta |_{\eta=1} = 0$.

2.2. Analytical Solutions and Experimental Procedure

A solution of Equation 4 for a point source injection located at (x_k, η_k) in a laterally confined channel is expressed as a summation of $4N + 1$ virtual sources located beyond the bank:

$$D(x, \eta) = \frac{D(x_k, \eta_k) \times Q}{\sqrt{4\pi B(x - x_k)}} \exp\left[-\frac{Q^2(\eta \pm \eta_k)^2}{4B(x - x_k)}\right] + \sum_{n=1}^N \frac{D(x_k, \eta_k) \times Q}{\sqrt{4\pi B(x - x_k)}} \exp\left[-\frac{Q^2(2n \pm \eta \pm \eta_k)^2}{4B(x - x_k)}\right] \quad (5)$$

The diffusion factor $B_{k,i}$ of the sub-reach located between the tracer injection point at (x_k, η_k) and the measurement cross-section at x_i (cf. Figure 1) is estimated through the best-fitting of Equation 5 against

the dosage profile $D(x_i, \eta)$ measured at the downstream cross-section, knowing the dosage $D(x_k, \eta_k)$ at the injection point.

On the other hand, to estimate the diffusion factor $B_{i,i+1}$ of the sub-reach located between two consecutive measurement cross-sections located respectively at x_i and x_{i+1} (cf. Figure 1) downstream of the injection point, the analytical solution of Equation 4 for a tracer source distributed across the upstream cross-section must be used:

$$D(x_{i+1}, \eta) = \frac{1}{N_j} \sum_{j=1}^{N_j} \left(\frac{D(x_i, \eta_j) \times Q}{\sqrt{4\pi B_{i,i+1} (x_{i+1} - x_i)}} \exp \left[\frac{-Q^2 (\eta \pm \eta_j)^2}{4B_{i,i+1} (x_{i+1} - x_i)} \right] + \sum_{n=1}^N \frac{D(x_i, \eta_j) \times Q}{\sqrt{4\pi B_{i,i+1} (x_{i+1} - x_i)}} \exp \left[\frac{-Q^2 (2n \pm \eta \pm \eta_j)^2}{4B_{i,i+1} (x_{i+1} - x_i)} \right] \right) \quad (6)$$

In such case, the upstream dimensionless dosage cross-profile computed at section x_i using Equation 5 is discretized in $N_j = 100$ values at positions $\eta_j = j / N_j$ separated by constant discharge increments $1 / N_j$ (cf. Figure 1d). The diffusion factor $B_{i,i+1}$ of the sub-reach between cross-sections at x_i and x_{i+1} is then estimated through the best-fitting of Equation 6 against the dosage profile $D(x_{i+1}, \eta)$.

This procedure is cost-efficient since a single slug injection at x_k yields transverse mixing coefficient estimates for two consecutive sub-reaches (x_k, x_i) and (x_i, x_{i+1}) , provided that the concentration profiles at both cross-sections x_i and x_{i+1} can be recorded simultaneously. Repeating this procedure in various sub-reaches allows assessing the longitudinal variation of the diffusion factor and thus the transverse mixing coefficient.

2.3. Longitudinal Flow Nonuniformity Parameters

A flow is considered nonuniform when the streamwise profiles of the water surface elevation $z_w(x)$ and of the hydraulic head $E(x) = z_w + \bar{u}^2 / 2g$ (m) are not parallel, with \bar{u} (m/s) the transverse-averaged velocity and g (m²/s) the gravitational acceleration. To quantify such flow nonuniformity, Kironoto et al. (1995) introduced the equilibrium pressure-gradient parameter:

$$\beta = \frac{\bar{h}}{\tau_0} \frac{dp^*}{dx} \quad (7)$$

where $\tau_0 = \rho g \bar{h} S_E$ is the bottom shear stress, \bar{h} the transverse-averaged water depth, $S_E = -dE / dx$ the local head slope or head loss, and $dp^* / dx = -\rho g S_w$ the longitudinal pressure gradient with $S_w = -dz_w / dx$ the slope of the water surface elevation. The parameter β is simply the opposite of the water surface elevation slope to head slope ratio:

$$\beta = -\frac{S_w}{S_E} \quad (8)$$

In an accelerating flow, the velocity increases ($d\bar{u} / dx > 0$) so that the head slope is milder than the water surface elevation slope and $\beta < -1$. Oppositely, in a decelerating flow, the velocity decreases ($d\bar{u} / dx < 0$) so that the head slope is greater than the water surface elevation slope and $\beta > -1$. The uniform flow condition corresponds to $\beta = -1$ since both slopes are equal. However, when a succession of accelerating, decelerating or relatively uniform flows occurs along a river reach, an average β value does not capture the flow non-uniformity. Indeed, the reach-averaged equilibrium pressure-gradient parameter is computed as the length-weighted average value $\beta = (1 / X) \sum X_n \beta_n$, where β_n and X_n are the local equilibrium pressure-gradient parameter and length, respectively, of the n^{th} sub-reach ($X = \sum X_n$). Consequently, local β_n smaller and greater than -1 may cancel each other so that $\beta \sim -1$, suggesting that overall the flow is uniform. We thus

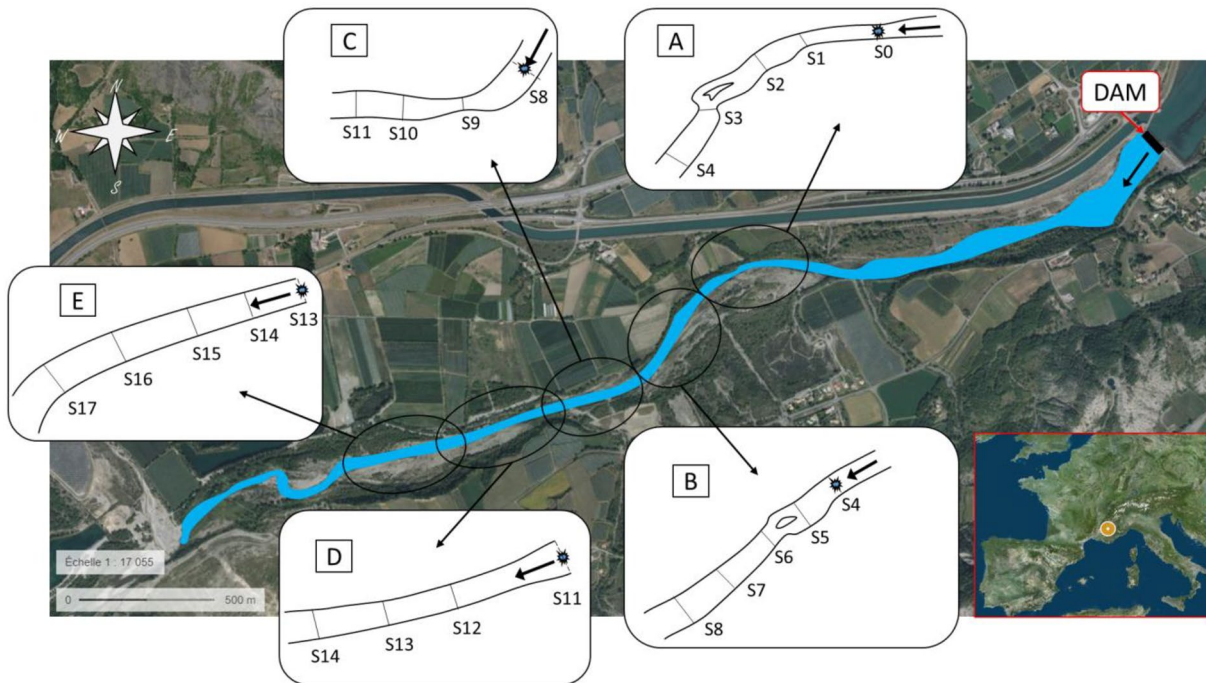


Figure 2. Layout of the study reach of the Durance at La Saulce, France, delineated in five zones A, B, C, D and E corresponding to the five injection points (S0, S4, S8, S11, 13) and in 17 sub-reaches. Black arrows show the flow direction (Source Geoportail: <https://www.geoportail.gouv.fr>).

propose a more representative indicator of flow nonuniformity (called here the nonuniformity parameter) along a river reach: $\kappa = (1/X) \sum X_n |\beta_n + 1|$. Since κ is the sum of positive or null values, it equals zero only if the flow is uniform in all sub-reaches. However, the distinction between accelerating and decelerating flows is lost when using κ instead of β .

Finally, the general expression ruling the transverse mixing coefficient derived from dimensional analysis (Equation 1) can be extended to include flow nonuniformity effects using parameter κ :

$$\frac{E_y}{LV} = f\left(\frac{U}{u_*}, \frac{W}{H}, S_n, \kappa\right) \quad (9)$$

An objective of the present work is to assess the influence of this fourth parameter and the potential for deriving a unique predicting equation covering both field and laboratory situations.

3. Experimental Work

3.1. Field Site

The experimental work is conducted in a 2 km-long segment of the Durance River (between 44°24'59.79"N 6°0'9.61"E and 44°24'35.02"N 5°58'58.23"E) near La Saulce, France (Figure 2) during a three-day campaign between 24/09/2019 and 27/09/2019. The Durance River is a piedmont river flowing from the French Southern Alps to the Rhône River. This river is subject to Mediterranean flash floods that drastically change its morphology. The study reach is by-passed by a hydropower canal so that the discharge released from the dam remains constant during our experiments. All along the campaign, the discharge measured at several cross-sections using a 2,400 kHz Teledyne RDI StreamPro Acoustic Doppler Current Profiler (ADCP) is 5.3 m³/s on average with a standard deviation of 0.4 m³/s (~8%). The river reach can be seen as a longitudinal succession of sub-reaches with different types of roughness elements, such as channels bedded with sand, rocks (pebbles or bigger rocks), and emerging obstacles, as presented below.

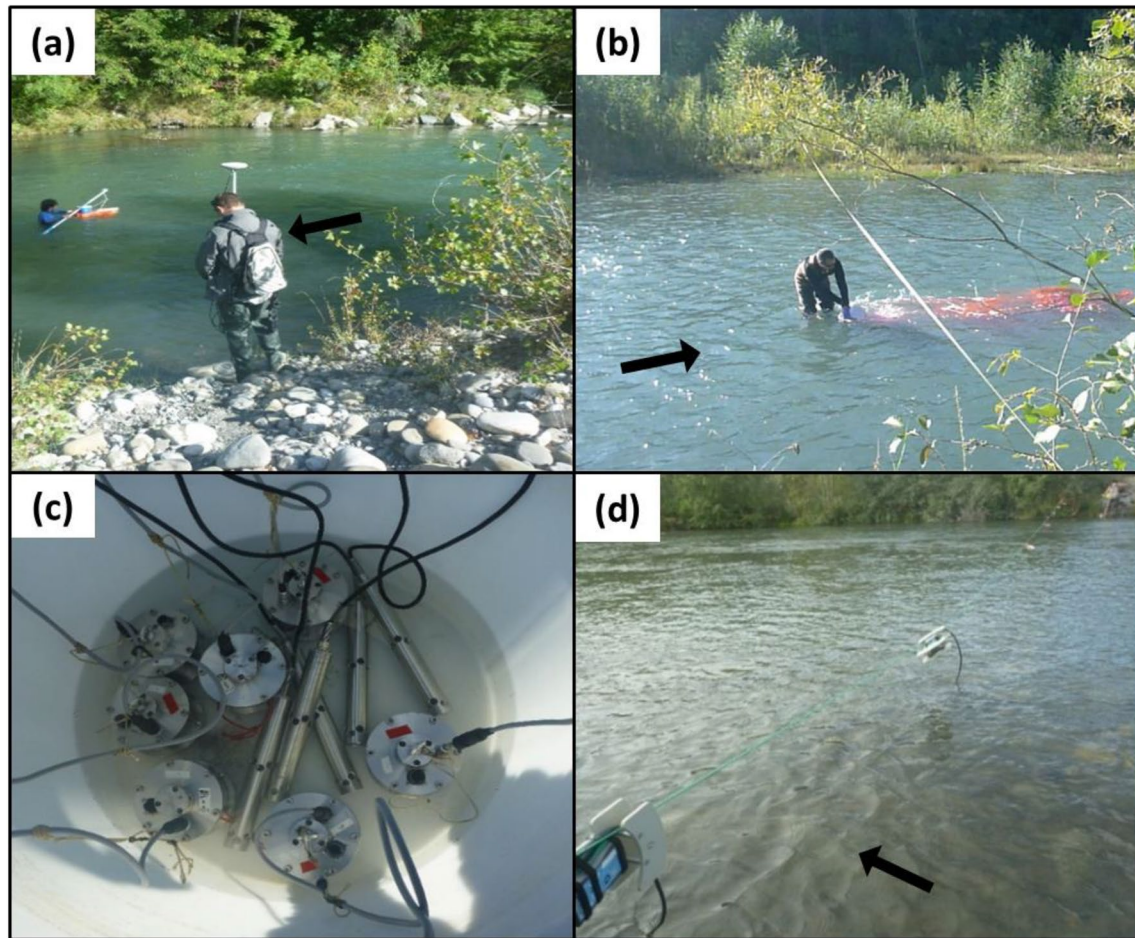


Figure 3. Instruments and their deployment: (a) ADCP and DPGS measurements at cross-section S1.5, (b) injection of tracer at cross-section S13, (c) the fluorimeters (7 Albillia and 5 TQ tracers) deployed in the calibration tank and (d) along cross-section S10. Black arrow indicate the flow direction.

3.2. Measurement Methods and Equipment

The streamtube version of the 1D diffusion model (cf. Section 2.1) requires that concentration measurements are positioned at known cumulative discharge values across each measurement cross-section. Also, the reach-averaged velocity-shape factor Ψ , water depth H , channel width W and velocity U of each sub-reach must be evaluated.

The depth-averaged velocity u and water depth h are measured along different cross-sections bordering and within the sub-reaches using a Teledyne RDI StreamPro 2,400 kHz ADCP mounted on a little float as shown in Figure 3a. The float and the ADCP are moved from bank to bank by a wading operator or from an inflatable boat in the deepest areas. The streamwise profile of water surface elevation $z_w(x)$ is measured using a Leica DGPS System 1200 with RTK correction from the Orpheon network (cf. Figure 3a).

The tracer used for slug injections (cf. Figure 3b) is liquid Rhodamine WT 20%, a fluorescent tracer with high detectability and low toxicity. Seven GNU-FL30 Albillia sensors and five TQ-tracers (Sommer Messtechnik) record the water fluorescence with a sampling frequency of 2–3 Hz for the Albillia and 1 Hz for the TQ tracers. All the fluorimeters (Albillia and TQ-tracers) are calibrated every day after the tracing experiments to relate the voltage response to the actual concentration of Rhodamine WT. To do so, precise doses of Rhodamine WT are injected in a big tank filled with river water (cf. Figure 3c) to increase the concentration by increments of 10 ppb, reaching 0, 10, 20, 40, 80 and 160 ppb. The temperature of the flow is measured every minute with a micro-Diver (SWS Technology) during the tracing experiment in order to correct the fluorescence signal as proposed by Poncet (2017):

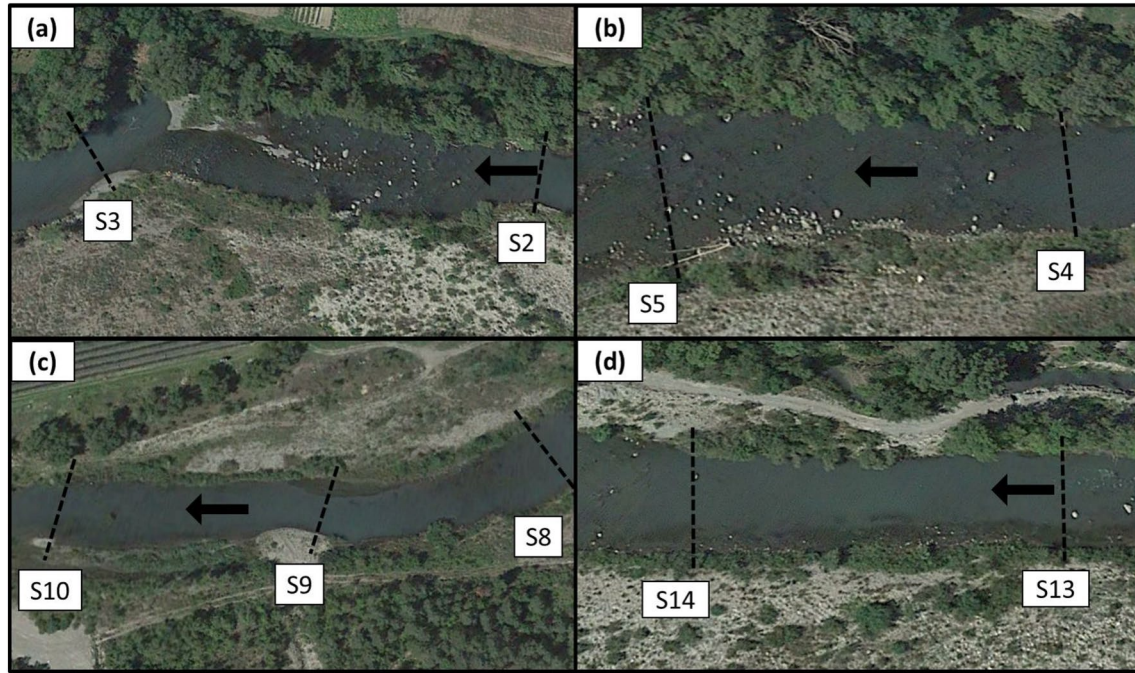


Figure 4. Examples of studied sub-reaches with variable bed morphology: (a) a complex riffle for S2-S3, (b) emerging blocks for S4-S5, (c) a pebble bed with a mild meander for S8-S9 et S9-S10, (d) a sand bedded straight channel for S13-S14.

$$F_{corr} = F_{meas} \times e^{n(T_{cal} - T_{meas})} \quad (10)$$

where F_{meas} and T_{meas} are respectively the fluorescence and temperature in the water measured during the injection experiments, T_{cal} is the temperature of the water during the calibration process, and n is a coefficient depending on the type of fluorimeter: $n = 0.026$ for Albillia sensors, and $n = 0.021$ for TQ-tracers.

3.3. Delineation of the Sub-reaches and Hydraulic Parameters

The strategy consists of splitting the 2-km long river reach in 17 sub-reaches and conducting tracing experiments in each sub-reach. ADCP measurements are performed at 29 cross-sections, including the 18 cross-sections bordering the sub-reaches (cf. Figure 2). Sub-reaches are labeled by their limiting cross-sections, e.g., sub-reach S0-S1 is delineated by cross-sections S0 and S1, etc. The remaining 11 cross-sections are referred to as “intermediate cross-sections” and are positioned near the middle of the sub-reaches: for instance, cross-section S0.5 is an intermediate cross-section located within sub-reach S0-S1, i.e., between cross-sections S0 and S1.

During the campaign, the injection point is regularly moved downstream in order to minimize the risk of perfectly mixed tracer in the transverse direction, which would prevent the estimation of the transverse mixing coefficient. Therefore, the study site is divided in five injection zones (cf. Figure 2). Injections are performed at the center of cross-sections S0, S4, S8, S11 and S13, corresponding to injection zones A to E. For each injection, two consecutive fluorescence measuring cross-sections (noted S_i and S_{i+1} in Figure 1) are equipped with six fluorimeters each placed on the bed (cf. Figure 3d) at equal discharge increments ($= 1/7, \dots, 6/7$) measured by the ADCP. The Albillia sensors are located near the center of the cross-sections where peak concentrations are the highest while TQ-tracers are located near the banks due to their higher sensitivity and lower saturation level.

Figure 4 shows photographs of selected sub-reaches, revealing very different river aspects. The sub-reaches delineation is somehow subjective but it is mainly based on eye-identification of roughness elements and bed morphology. Each macro-scale obstacle such as a riffle, an island or a patch of emerging blocks is

Table 1
Hydraulic Data at Each Cross-Section

Cross-section	X (m)	ψ (-)	w (m)	\bar{h} (m)	\bar{u} (m/s)	z_w (m)	E (m)
S0	0	1.14	16.7	0.69	0.46	560.520	560.531
S0.5	34	1.11	13.6	0.42	0.93	560.310	560.354
S1	101	1.77	13.6	0.49	0.79	559.795	559.827
S1.5	141	2.27	13.7	0.97	0.40	559.791	559.799
S2	156	-	-	-	-	559.761	-
S3	306	2.00	14.3	0.95	0.39	558.865	558.873
S3.5	337	1.19	22.3	0.73	0.32	558.864	558.869
S4	371	1.13	24.4	0.52	0.42	558.86	558.869
S5	444	1.18	31.6	0.33	0.50	558.549	558.562
S6	544	1.88	17.9	0.77	0.39	557.391	557.399
S7	629	1.10	18.2	1.14	0.25	557.36	557.363
S8	762	1.44	29.8	0.43	0.42	557.349	557.358
S8.5	820	1.89	23.0	0.46	0.50	557.190	557.203
S9	863	1.10	18.9	0.72	0.39	557.171	557.179
S9.5	901	1.22	24.8	0.46	0.46	557.156	557.167
S10	980	1.07	24.4	0.43	0.50	557.061	557.074
S10.5	1,010	1.05	25.4	0.52	0.40	556.969	556.977
S11	1,077	1.01	22.2	0.43	0.56	556.623	556.639
S11.5	1,249	1.18	18.4	0.34	0.85	556.380	556.417
S12	1,307	1.11	20.0	0.48	0.55	555.937	555.953
S13	1,400	1.39	19.4	0.70	0.39	555.035	555.043
S13.5	1,439	1.07	19.3	0.70	0.39	555.034	555.042
S14	1,465	1.05	20.1	0.58	0.45	555.014	555.025
S14.5	1,588	1.74	24.2	0.36	0.60	554.664	554.683
S15	1,626	1.03	25.1	0.49	0.43	554.514	554.523
S15.5	1,700	2.05	28.7	0.36	0.51	554.350	554.363
S16	1,780	1.01	25.6	0.43	0.49	554.017	554.029
S16.5	1,822	1.72	16.2	0.57	0.57	553.910	553.927
S17	1,859	1.12	21.2	0.36	0.69	553.838	553.862

systematically included near the middle of a sub-reach. Moreover, each sub-reach has to be sufficiently long (>50 m) so that dosage cross-profiles recorded at successive cross-sections with a limited number of probes are sufficiently different to allow an accurate estimation of the transverse mixing coefficient of the sub-reach through fitting of the advection-diffusion model (Equations 5 and 6).

The studied reach comprises four riffles sub-reaches: S2-S3 (cf. Figure 4a), S5-S6, S10-S11 and S12-S13. The first two are located within a complex channel, with emerging blocks upstream followed by an island dividing the riffle in two flows. These two flows merge further downstream in a curved channel where the water depth strongly increases. The other two riffles exhibit a simpler morphology, with a straight channel, a typically high slope and a low water depth.

Emerging blocks are observed within reaches S0-S1, S4-S5 (cf. Figure 4b), S14-S15 and S15-S16. Sub-reaches S0-S1 and S15-S16 are composed of an upstream region with large immersed boulders and a downstream region with smaller emerging blocks.

Sub-reaches S7-S8, S8-S9, S9-S10, S11-S12 and S16-S17 are rough channels with medium-sized pebbles ($d_{50} \sim 0.1H$). Moreover, sub-reaches S8-S9 and S9-S10 exhibit complex topographical variations: the water depth increases along the left bank for sub-reach S8-S9, while the opposite holds for S9-S10. Cross-section S9 is located at the throat of an S-shaped section of the channel (cf. Figure 4c).

Sub-reaches S1-S2, S3-S4, S6-S7 and S13-S14 (cf. Figure 4d) are mild slope sand-bedded sub-reaches mostly located just downstream from riffles with a bed covered with sand and small gravels ($d_{50} \sim 0.01H$). They exhibit the largest water depth ($H > 0.5$ m, up to $H \sim 1$ m for S6-S7). The width of the channel in sub-reach S1-S2 increases after S1 and recirculation zones are present on each side of the channel.

Table 1 summarizes the hydraulic characteristics of each cross-section. The overbar represents a cross-sectional averaged, and the lower case w and ψ are the width and velocity-shape factor of the corresponding cross-section respectively. These hydraulic quantities substantially vary over the whole domain, as depicted on Figure 5. The four sudden water surface elevation drops in in Figure 5a are due to the four riffles located at $X \sim 250, 500, 1050$ and 1350 m downstream from cross-section S0. Just downstream from the riffles, the bed slope strongly decreases while water depth increases, until the next riffle.

The sub-reach averaged hydraulic and geometric parameters $H, W, U, u_*, \Psi, \lambda, W/H, \beta$ and κ are listed in Table 2. These values are obtained by averaging the consecutive cross-sectional averaged values included at the border of each sub-reach and within each-reach for those containing an intermediate cross-section, using a length-weighted-average in the same way as in Section 2.3.

3.4. Tracing Experiments

For each injection, the dosage cross-profiles are fitted using the procedure described in Section 2.2 with an example in Figure 6b for the slug injection at section S13 and measurements at sections S14 and S15. For all injections, Table 2 summarizes the fitted diffusion factors B and the corresponding transverse mixing coefficient E_y .

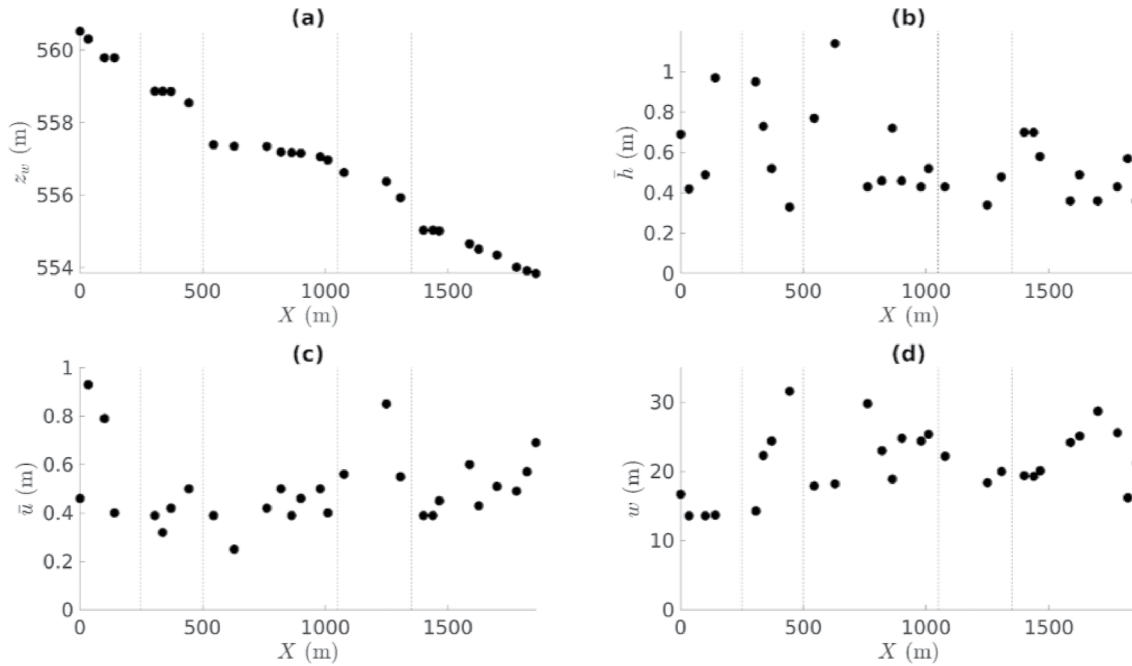


Figure 5. Longitudinal evolution of the hydraulic parameters measured along the study reach from cross-section S0 ($X = 0$): (a) water surface elevation z_w , (b) cross-sectional averaged water depth \bar{h} , (c) cross-sectional averaged velocity \bar{u} , (d) river width w . Riffles are indicated by vertical blue dash lines.

To assess the repeatability of the tracing experiments, the dosage measurements at cross-sections S2, S3, S6, S7, S10, S11, S12, S13, S15, and S16 are repeated twice with the same injection point. For example, the repeated dosage cross-profile measurements at S15 (cf. Figure 6b) with injection at S13 show the relatively good agreement. Moreover, the diffusion factor of sub-reach S13-S14 is estimated twice: with an injection at S11 (zone D in Figure 2) and a with a closer injection at S13 (zone E). The resulting diffusion factors are found identical (cf. column #17 in Table 2).

Unfortunately, two cases of perfect mixing are reported: for the injections at S0 (zone A) and at S4 (zone B), the tracer is almost perfectly mixed at cross-sections S3 and S7, respectively. Consequently, the transverse mixing coefficients for sub-reaches S3-S4 and S7-S8 could not be estimated. These results confirm that dividing the domain in at least five injection zones (A, B, C, D and E, see Figure 2) for consecutive injections was required. Moreover, the measured dosage cross-profiles hardly evolve between monitored sections S10 and S11, within the range of the measurement uncertainties. Here again, no diffusion factors and mixing coefficients could be estimated, but are expected to be “very low”. Finally, since the hydraulic data at S2 is not available (due to experimental limitation, see Table 1), the diffusion factors for S1-S2 and S2-S3 could be estimated but not the corresponding transverse mixing coefficients.

4. Results

4.1. Influence Factors for the Transverse Mixing Coefficient

Present section analyses the measured dimensionless mixing coefficient $E_y / (LV)$, where V can be selected as the sub-reach averaged u_* (friction velocity) or U (bulk velocity) and L as W (channel width) or H (water depth). The measured transverse mixing coefficient given in Table 2 and plotted in Figure 7a and Figure 7b is found to vary quite substantially within the studied domain, with a weight-average of $E_y / (Hu_*) = 0.48$ and $R^2 = 40\%$, corresponding to the gently meandering channel configuration following Rutherford (1994). A minimum of $E_y / (Hu_*) = 0.2$ is obtained in a relatively straight channel with emerging obstacles (i.e., S4-S5), and a maximum of $E_y / (Hu_*) = 1.25$ is found in a straight sand channel (i.e., S13-S14) downstream of a riffle. The lowest value is in agreement with Rutherford (1994) for the straight channel case. The high-

Table 2
Characteristics of Each Sub-Reach Along With Computed Mixing Coefficients

Injection zone	Sub-reach	Roughness type	Length (m)	S_w (m/km)	S_E (m/km)	W (m)	H (m)	W/H	U (m/s)	$u_* = \sqrt{gHS_E}$ (m/s)	λ	Ψ	β	κ	S_n	B (m ⁵ /s ²)	E_y (m ² /s)
A/S0 (Day 1)	S0-S1	Emerging blocks	101	7.17	6.97	14	0.49	28.8	0.80	0.18	0.41	1.33	-1.05	0.08	1.01	0.006	0.023
	S1-S2	Sand	55	-	-	-	-	-	-	-	-	-	-	-	1.02	-	-
	S2-S3	Riffle-island	150	-	-	-	-	-	-	-	-	-	-	-	1.12	-	-
	S3-S4	Sand	65	0.06	0.04	21	0.73	28.7	0.36	0.02	0.03	1.37	-6.75	6.42	1	^a	^a
B/S4 (Day 2)	S4-S5	Emerging blocks	73	4.28	4.22	28	0.42	65.9	0.46	0.13	0.66	1.16	-1.01	0.012	1	0.0011	0.011
	S5-S6	Riffle-island	100	11.58	11.63	25	0.55	45	0.44	0.25	2.54	1.53	-1	0.00	1.05	0.0141	0.069
	S6-S7	Sand	85	0.42	0.48	18	0.95	18.9	0.32	0.07	0.34	1.49	-0.89	0.12	1	0.014	0.032
	S7-S8	Rocks	133	0.08	0.04	24	0.78	30.6	0.34	0.02	0.02	1.27	-2.01	1.01	1.01	^a	^a
C/S8 (Day 2)	S8-S9	Rocks	101	1.76	1.77	24	0.51	47.3	0.45	0.09	0.31	1.59	-0.93	0.10	1.04	0.0064	0.035
	S9-S10	Rocks	117	0.94	0.90	24	0.50	47.8	0.46	0.06	0.15	1.15	-1.10	0.10	1.02	0.004	0.031
	S10-S11	Riffle	97	4.52	4.49	24	0.47	50.9	0.47	0.14	0.74	1.04	-1	0.00	1.01	Very low	Very low
D/S11 (Day 3)	S11-S12	Rocks	230	2.98	2.98	20	0.39	50.4	0.70	0.10	0.19	1.12	-1.04	0.08	1	0.0022	0.018
	S12-S13	Riffle	93	9.70	9.78	20	0.59	33.3	0.47	0.24	2.04	1.25	-0.99	0.01	1	0.005	0.024
	S13-S14	Sand	65	0.32	0.28	19	0.68	28.8	0.40	0.03	0.08	1.16	-1.10	0.10	1	0.0061	0.028
E/S13 (Day 3)	S13-S14	Sand	65	0.32	0.28	19	0.68	28.8	0.40	0.03	0.08	1.16	-1.10	0.10	1	0.0061	0.028
	S14-S15	Emerging blocks	161	3.11	3.11	23	0.46	49.4	0.53	0.12	0.40	1.39	-1	0.032	1.01	0.002	0.013
	S15-S16	Emerging blocks	154	3.23	3.21	27	0.41	66	0.48	0.11	0.43	1.54	-1.01	0.013	1.01	0.0013	0.010
	S16-S17	Rocks	79	2.27	2.11	20	0.48	41.1	0.58	0.10	0.26	1.39	-1.08	0.08	1	0.0029	0.015

-: missing values due to missing hydraulic data at S2.

^acases of perfect mixing.

est value would correspond to the sharply curved channel case in Rutherford's classification. Overall, no clear relation could be found between the morphology of the sub-reaches and the corresponding transverse mixing coefficients:

- The dimensionless mixing coefficient generally decreases with increasing friction factor λ , except for the two very high λ values, corresponding to the cases of riffle sub-reaches, i.e., S5-S6 and S12-S13 (cf. Figures 7c and 7d). Additionally, these exceed those obtained in laboratory channels for similar high values of friction coefficient ($E_y / (Hu_*) = 0.13$ for $\lambda > 0.08$).
- $E_y / (WU)$ and $E_y / (Wu_*)$ decrease with increasing aspect ratio (cf. Figure 7f).
- No clear trend with the sinuosity S_n (cf. Figures 7g and 7h) is found except for $E_y / (Hu_*)$, where a slight increase of the coefficient with increasing S_n is observed.

Overall, the present analysis does not permit to identify the governing parameters (i.e., λ , W/H , and S_n) ruling the longitudinal variability of dimensionless transverse mixing coefficient measured in the Durance River.

4.2. Predictive Equation Including Flow Nonuniformity

The ability of equations recently published by Aghababaei et al. (2017), Deng et al. (2001), Huai et al. (2018), and Jeon et al. (2007) to predict the measured transverse mixing coefficients is tested here. Four equations

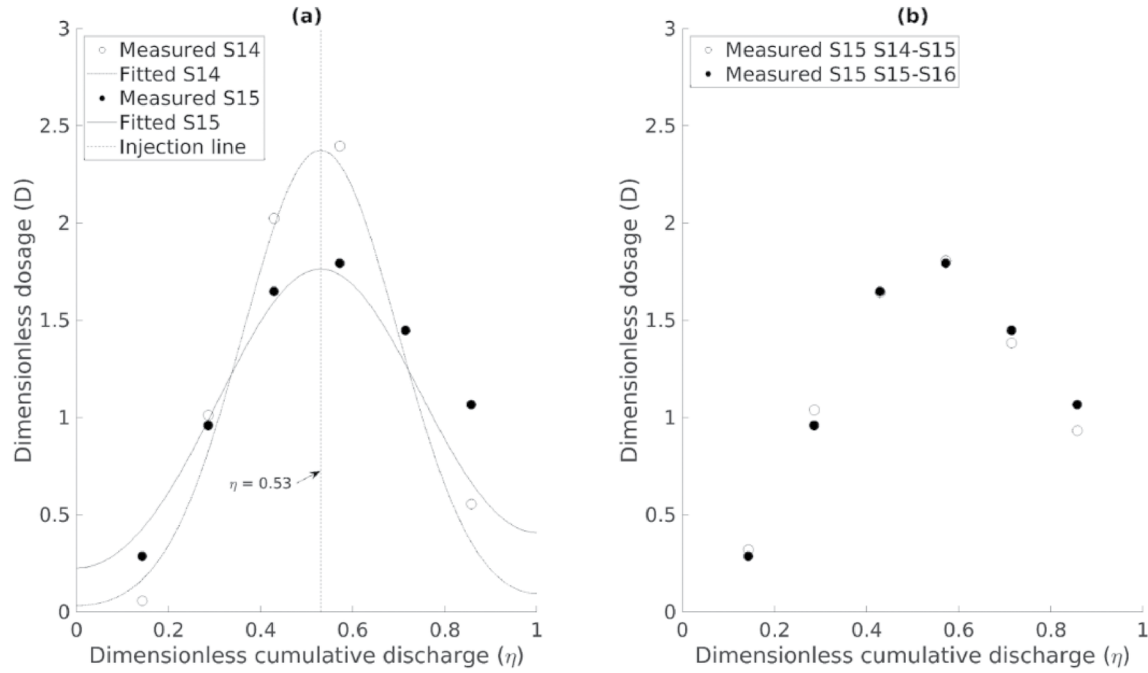


Figure 6. Examples of dimensionless dosage measurements and transverse mixing coefficient estimation: (a) fit of the diffusion model for sub-reach S14-S15 with injection at cross-section S13, (b) repeated dosage measurements at cross-section S15.

from recent literature are evaluated by comparison with our measurements. The parameters on which they are based are reported in Table 3 and short descriptions follow.

Deng et al. (2001) developed an equation for the longitudinal mixing coefficient based on Fischer et al. (1979) integral expression. This expression requires a transverse mixing coefficient, which the authors defined as the sum of two terms: a constant transverse turbulent diffusion term derived from Rutherford (1994) data collected in laboratory configurations, and a dispersion term that Smeithlov (1990) derived from river measurements in meandering channels: $E_y / (Hu_*) = 0.145 + (1 / 3520)(U / u_*)(W / H)^{1.38}$.

Jeon et al. (2007) derived an equation for natural streams based on three parameters (see Table 3) fitted on 16 flow configurations. An additional set of 16 cases was used to validate the proposed equation with a correlation coefficient of 78%. This equation does not differentiate the contributions of turbulent diffusion and dispersion, and considers the mixing coefficient as a product of powers of the different parameters: $E_y / (Hu_*) = 0.0291(U / u_*)^{0.46} (W / H)^{0.3} S_n^{0.73}$.

Aghababaei et al. (2017) proposed two equations using a multiple linear regression method and a genetic programming based symbolic regression calibrated on 181 cases. The authors argue that the latter is more accurate: $E_y / (Hu_*) = 0.463 + 0.464(U / u_*) + 8.8 \times 10^{-9} S_n^{(U / u_*)} + 0.15 S_n^{(U / u_*) + (2.3 F_r S_n^2) - 25.3} - 0.474 S_n^{0.054(W / H) - 20.37}$.

Finally, Huai et al. (2018) used a genetic programming based model to propose an equation for the transverse mixing calibrated on 39 flow cases in natural streams. Two terms in the equation reflecting turbulent diffusion and dispersion are first established from 147 laboratory data. Then coefficients are introduced to scale these two terms and fit the river cases: $E_y / (Hu_*) = \left(0.69(U / u_*)^{0.47} \right) / \left(262 + (U / u_*)^2 - 31.8(U / u_*) \right) + \left(0.12(W / H)^{1.07} (U / u_*)^{0.35} S_n^{0.395} \right) / \left((W / H) + 0.222(U / u_*) - 1.99 \right)$.

The values of the dimensionless transverse mixing coefficient $E_y / (Hu_*)$ predicted by each equation (cf. columns #3 to 6 in Table 3) vary strongly from one equation to another for the hydraulic and geometric conditions faced in present experiments in the Durance River (cf. Figure 8). They also present a poor agreement with the corresponding measured values of the transverse mixing coefficient (cf. column #2 in Table 3).

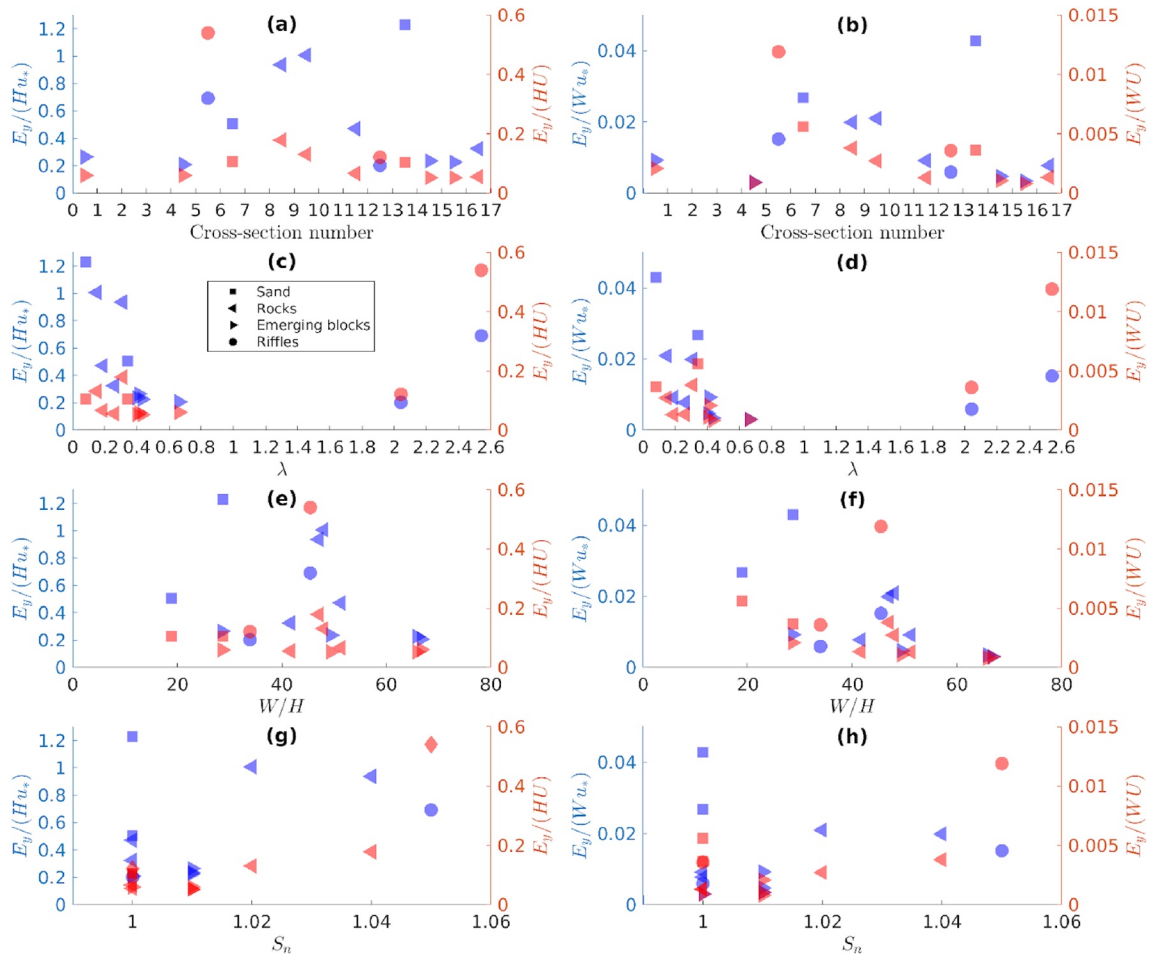


Figure 7. Plots of the dimensionless transverse mixing coefficient: (a and b) the longitudinal set of sub-reaches, (c and d) the sub-reach averaged friction factor, (e and f) the sub-reach averaged aspect ratio, (g and h) the sub-reach averaged sinuosity; blue and red symbols refer to the left axis ($V = u_*$) and the right axis ($V = U$), respectively.

In particular, all equations underestimate the highest measured values ($E_y / (Hu_*) > 0.4$). This analysis confirms that a major process governing the transverse mixing in piedmont rivers was omitted in the establishment of the previous predictive equations made by these authors.

Additionally, the formulations from the literature and Rutherford (1994) classification for straight channels are in agreement with the measured mixing coefficients when the flow nonuniformity factor is low. In most formulations, sinuosity is the only factor that may increase the mixing coefficient estimates, flow nonuniformity being always ignored. Since the sinuosity of the Durance River is negligible (S_n is close to 1) for the studied sub-reaches, the formulations from the literature strongly underpredict the highest observed mixing coefficients values.

As discussed above, we hypothesize that this parameter could be the parameter κ , reflecting for the longitudinal nonuniformity of the flow. The relation between the measured dimensionless transverse mixing coefficients and parameter κ is investigated in the following.

Since intermediate cross-sections were not monitored for the sub-reaches containing a riffle (S5.5 and S12.5 could not be measured in sub-reaches S5-S6 and S12-S13), the available hydraulic data do not correctly capture the streamwise flow variations within these sub-reaches, i.e., a rapid acceleration leading to very shallow water with strong slope, then a rapid deceleration in a deep pool. In such cases, the calculated parameter κ is not representative of the flow nonuniformity within the sub-reach. A more accurate

Table 3
Comparison of the Dimensionless Transverse Mixing Coefficient Between Results of This Study and Prediction From Literature's Equations

		Predictive equations for $E_y / (Hu_*)$				
Parameters involved		Deng et al. (2001)	Jeon et al. (2007)	Aghababaei et al. (2017)	Huai et al. (2018)	Equation 12
		U / u^*	$U / u^* \in [2;12]$	$U / u^* \in [4.5;23]$	$U / u^* \in [3.7;24]$	$U / u^* \in [4;13]$
		W / H	$W / H \in [10;110]$	$W / H \in [2.5;287]$	$W / H \in [14;170]$	$W / H \in [18;66]$
			$S_n \in [1;2.1]$	$S_n \in [1;3.3]$	S_n	$\kappa \in [0;0.12]$
				$F_r \in [0.06;0.58]$		
Sub-reach	Measured	Predicted				
S0-S1	0.26	0.28	0.16	0.23	0.28	0.29
S4-S5	0.2	0.5	0.19	0.21	0.26	0.13
S6-S7	0.51	0.23	0.15	0.16	0.28	0.54
S8-S9	0.79	0.46	0.21	0.31	0.31	0.77
S9-S10	0.99	0.61	0.24	0.24	0.35	1.17
S11-S12	0.44	0.57	0.23	0.14	0.33	0.52
S13-S14	1.25	0.44	0.25	0.14	0.45	1.02
S14-S15	0.24	0.45	0.19	0.22	0.29	0.15
S15-S16	0.23	0.56	0.2	0.22	0.29	0.13
S16-S17	0.32	0.44	0.2	0.15	0.31	0.43

description of the longitudinal evolution of the hydraulic parameters would be required and the analysis of these two sub-reaches is discarded.

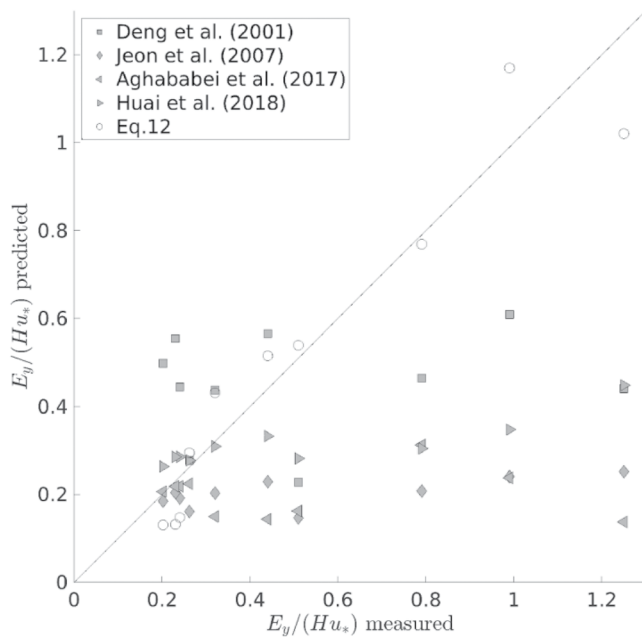


Figure 8. Comparison of the values predicted by several equations (including Equation 12 of this study) for the dimensionless mixing coefficient against the measured values in the Durance River.

We assume that the contribution of flow nonuniformity adds to the pre-existing mixing in the corresponding uniform flow conditions. Since the friction coefficient is relatively large in each sub-reach ($\lambda > 0.08$, cf. Table 2), the transverse mixing coefficient in corresponding uniform flow conditions would equal $E_y = 0.13Hu_*$, following the analysis of Weibel and Schatzmann (1984) as discussed in the introduction section. The values of $(E_y - 0.13Hu_*) / (LV)$ increase with the nonuniformity parameter κ for each selection of L and V (cf. Figure 9): the less uniform the flow is, the higher the dimensionless mixing coefficient is. This trend does not seem to depend on whether the flow accelerates, decelerates or goes through both an acceleration and a deceleration within a sub-reach. The contribution of flow nonuniformity is finally searched as a power function of κ as it should equal 0 when $\kappa = 0$ (uniform flow). The power functions are fitted in Figure 9 using a least squares method, and the adjustment for each cases of L and V is given as follows:

$$\frac{E_y - 0.13Hu_*}{Hu_*} = 4.65\kappa^{0.9}, R^2 = 43\% \quad (11a)$$

$$\frac{E_y - 0.13Hu_*}{HU} = 2.2^{1.4}, R^2 = 50\% \quad (11b)$$

$$\frac{E_y - 0.13Hu_*}{Wu_*} = 3.56\kappa^{2.3}, R^2 = 56\% \quad (11c)$$

$$\frac{E_y - 0.13Hu_*}{WU} = 2.6\kappa^3, R^2 = 90\% \quad (11d)$$

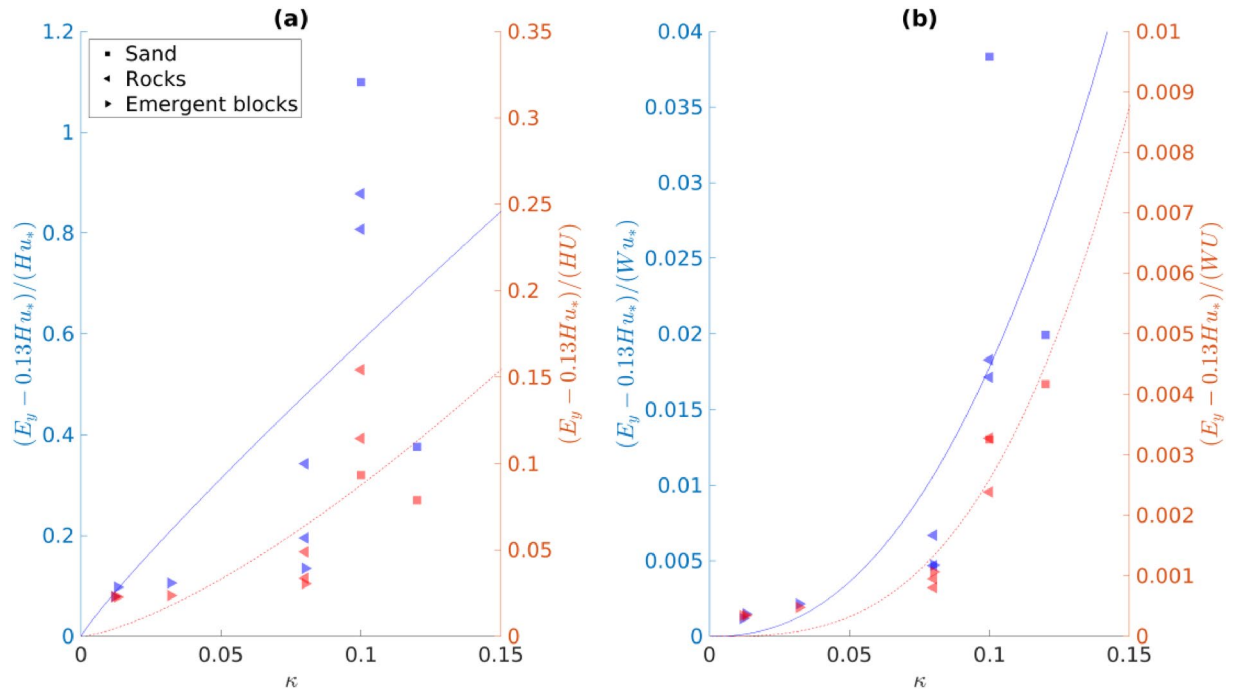


Figure 9. Excess dimensionless mixing coefficients $(E_y - 0.13Hu_*) / LV$ against the flow nonuniformity factor κ with: (a) $L = H, V = u_*$ or $V = U$, (b) $L = W, V = u_*$ or $V = U$ along with power function fits. Blue symbols and solid lines refer to the left axes ($V = u_*$), while red symbols and dashed lines refer to the right axes ($V = U$).

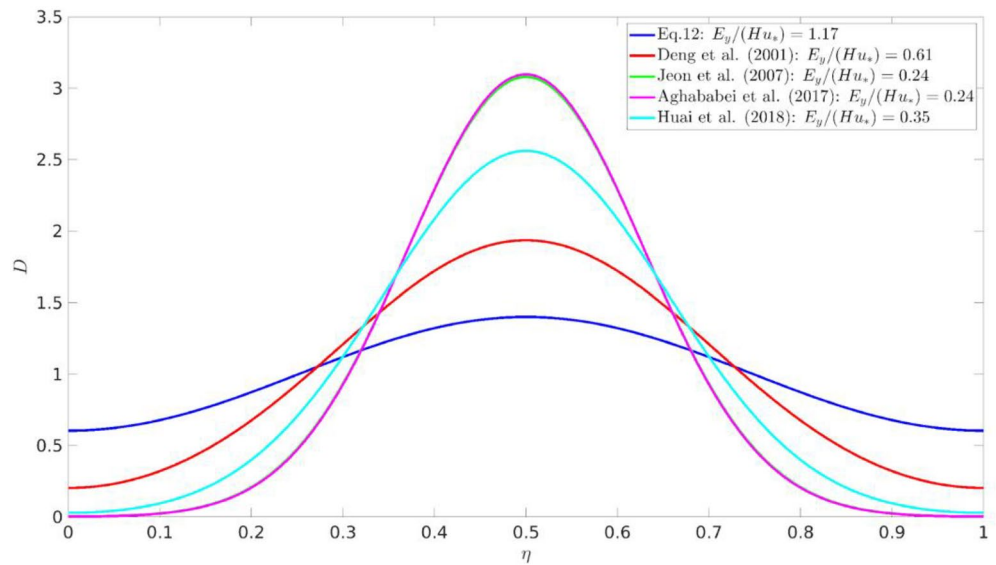


Figure 10. Dimensionless dosage profiles predicted for a hypothetical case based on the hydraulic conditions of S9-S10 sub-reach with $\kappa = 0.1$ and at $X = 10W$ from a point injection at the center of the flow ($\eta = 0.5$). Transverse mixing coefficient values are estimated using various formulations.

The best adjustment is then obtained for $V = U$ and $L = W$ (cf. Figure 9b, red symbols) in Equation 11d. A general equation for the typical dimensionless transverse mixing coefficient (i.e., $L = H$ and $V = u_*$) is thus proposed:

$$\frac{E_y}{Hu_*} = f(\lambda) + (2.6\kappa^3) \frac{W}{H} \frac{U}{u_*} \quad (12)$$

with $f(\lambda)$ a function of the friction coefficient equal to 0.13 when $\lambda > 0.08$. The apparently good agreement of Equation 12 with the experimental data available on the 10 sub-reaches is shown in Figure 8 (cf. column #7 in Table 3). The regression coefficient is good ($R^2 = 90\%$) but based on 10 calibration points only. This first evidence is encouraging but more measurements are required to validate the proposed equation.

5. Discussion

5.1. Why Does Mixing Efficiency Increase in a Nonuniform Flow?

The previous analysis reveals that the transverse mixing and the associated transverse mixing coefficient increases when the flow deviates from uniformity ($\kappa > 0$). The contribution of the flow nonuniformity is determined with a κ -dependent coefficient scaling the product WU in Equation 11d. The associated contribution to the mixing is thus a large-scale process with the river width as characteristic length, and the bulk velocity as characteristic velocity, typically large-scale secondary currents. It is interesting to note that the product of the aspect ratio and friction ratio in Equation 12, which naturally arises from this analysis, is also present in other predictive equation such as Deng et al. (2001) and Jeon et al. (2007) but with different exponents (e.g., $(U/u_*)(W/H)^{1.38}$ for Deng et al., 2001; $(U/u_*)^{0.46}(W/H)^{0.38}$ for Jeon et al., 2007). In the case of Jeon et al. (2007), the scaling coefficient is a function of the sinuosity.

The physical process that permits to increase the mixing efficiency as the flow becomes nonuniform appears symmetrical for both accelerating and decelerating flows. The longitudinal gradient of the bulk velocity seems to be generating the added mixing with a transverse redistribution of the mean streamwise velocities within the flow section, although it is not clear how.

First, Kironoto et al. (1995), and later Song and Chiew (2001), reported that the turbulent intensities tend to increase with increasing parameter β (i.e., flow deceleration). The increase of turbulent kinetic energy due to the decrease of the main flow kinetic energy could thus be an explanation of the increased mixing in decelerating flows.

Second, Yang et al. (2006), and Yang and Chow (2008) observed that the velocity dip, i.e., a minimum of the vertical profile of streamwise velocity below the free-surface, is increased in an accelerating flow. Such velocity dips are related to secondary current structures, as observed from experiments in laboratory flumes (Nezu & Nakagawa, 1984) and in natural reaches (Nezu et al., 1993). Therefore, stronger secondary currents may be the cause for the increased transverse mixing in accelerating flows.

5.2. Limitations of the Proposed Equation

Equation 12 is established in rough ($\lambda > 0.08$), straight ($S_n = 1$) river reaches. The contribution of flow nonuniformity to the mixing efficiency is added to the background mixing coefficient in uniform flow conditions, i.e., $E_y / (Hu_*) = 0.13$. The uncertainty of the nonuniformity parameter κ will depend on the quality of the hydraulic and water surface elevation measurements as well as the delineation of the studied reach. The proposed formula was determined for values of κ that are quite small, i.e., from 0 to 0.12. These values are obtained from measurements generally made at three cross-sections in a sub-reach: at both ends and at an intermediate cross-section. Nonetheless, in some cases practical limitations reduced the measurements to only the cross-sections at both ends of the sub-reaches. The value of the parameter κ is critical for applying Equation 12; it is yet not clear whether this equation still holds using more refined measurements, i.e., more intermediate cross-sections which would result in a more accurate value of κ . More data are required to explore this idea.

At lower friction coefficient ($\lambda < 0.08$), Weibel and Schatzmann (1984) showed that the transverse mixing coefficient depends on λ . For a wider applicability of Equation 12, the influence of λ , i.e., $f(\lambda)$ in Equation 12, should be defined over the full range of λ in an improved version of Equation 12.

5.3. Effect of Emerging Blocks

Fischer and Hanamura (1975) reported that, the transverse mixing coefficient $E_y / (Hu_*)$ is higher in a flow with emerging obstacles for $\lambda < 0.3$. Unfortunately, in present sub-reaches with emerging obstacles (i.e., S0-S1, S4-S5, S13-S14 and S14-S15) the friction factor always exceeds 0.3 (cf. Table 2), which prevents from possible comparisons with Fischer and Hanamura (1975) data. For three of sub-reaches with emerging blocks (i.e., S4-S5, S14-S15 and S15-S16) with the smallest values of κ (cf. Table 2 and Figure 8), the transverse mixing coefficient appears slightly underestimated by Equation 12. This may be explained by an underestimation of the nonuniformity parameters in these sub-reaches due to the difficulties of measuring the hydraulic parameters at cross-sections that would properly describe the longitudinal variations in sub-reaches containing emerging blocks.

5.4. Effect of the Sinuosity

Finally, the transverse mixing coefficient is expected to increase in highly sinuous rivers due to the increasing influence of the secondary currents, as described by Fischer (1969) for a single bend and by Baek et al. (2006) for successions of bends at low aspect ratio W / H . Fischer (1969) derived an equation for the dimensionless transverse mixing coefficient $E_y / (Hu_*)$ considering the product $(U / u_*)^2 (H / R_c)^2$. Later, Yotsukura and Sayre (1976) and Sayre (1979) proposed that an equation with better agreement using $(U / u_*)^2 (W / R_c)^2$. Nevertheless, Seo et al. (2016) showed that $E_y / (Hu_*)$ is only weakly related to the parameter $(U / u_*) (W / R_c)$, with an exponent of 0.35 as opposed to 2 proposed by Yotsukura and Sayre (1976) and Fischer (1969), and no clear relation is found between $E_y / (Hu_*)$ and W / R_c alone. Thus, the contribution of the sinuosity to the transverse mixing in rivers with large aspect ratio is still unclear. Future experiments in sinuous uniform and nonuniform reaches would be useful to assess the sole impact of the river sinuosity on the transverse mixing in order to include parameter S_n in Equation 12.

5.5. Practical Use of the Proposed Formula

Transverse mixing coefficients in rivers with longitudinally varied morphology, i.e., with successions of riffles and pools and changes of slope and roughness, appear strongly affected by the longitudinal nonuniformity of the flow. In practice, the presence of longitudinal nonuniformity seems to increase the transverse mixing coefficient. The difference in using Equation 12 rather than the equations available in the literature (that ignore the effect of nonuniformity factor) can be illustrated through a hypothetical case based on the hydraulic conditions of sub-reach S9-S10 (cf. Table 2) with high nonuniformity factor ($\kappa = 0.1$). Figure 10 shows the dimensionless dosage profiles predicted using various transverse mixing coefficient estimates. The profiles are calculated at a distance equal to 10 times the channel's width ($X / W = 10$) from a point injection at the center of the flow ($\eta = 0.5$). Equation 12 provides a much higher transverse mixing coefficient (cf. Table 3) due to the high value of parameter κ so that the resulting dosage profile would be much more flattened across the river cross-section than using the literature formulations. Consequently, the literature formulations would predict a much longer distance for complete mixing than the proposed formulation (Equation 12).

6. Conclusion

This experimental study involved tracing experiments performed in consecutive homogeneous sub-reaches of a 2 km-long reach of the Durance River. The chosen reach presented a substantial longitudinal variability of the morphology and flow nonuniformity. The application of the 1D streamtube diffusion model adjusted on measured dosage cross-profiles at cross-sections delineating the sub-reaches permitted to establish the longitudinal variability of the transverse mixing coefficient in the studied reach. However, the morphology

of the sub-reaches (riffle, emerging blocks, pools, and island) did not permit to explain the strong variability of measured transverse mixing coefficients, and existing formulas in the literature showed a poor capacity in predicting these coefficients.

Measurements of velocities and water depths along cross-sections, coupled with water-surface elevation measurements permitted to determine the longitudinal evolution of the hydraulic parameters, including the nonuniformity factor. The deviation from flow uniformity within the sub-reaches appears to be dominant in the tracer spreading efficiency, whether the flow is accelerated or decelerated. The inclusion of a parameter quantifying the flow nonuniformity (parameter κ) in the predictive equation for the transverse mixing coefficient proved to strongly improve the agreement between the predicted and measured transverse mixing coefficients. This new equation (Equation 12) seems particularly suitable to all sub-reaches with sufficiently large aspect ratio and friction coefficient, and with complex morphological patterns and successions of accelerating and decelerating flows. Unfortunately, no comparison with the literature data could be performed due to a lack of available information on the longitudinal nonuniformity in published datasets. Future tracing experiments will thus need to register the spatial distribution of the hydraulic and geometric parameters in order to validate the established equation, identify its limitations and add the contribution of other processes to the mixing efficiency, such as the stream sinuosity, the presence of emerging blocks or a limited friction coefficient. Additionally, a study involving a 2D model of the advection-diffusion equation could determine both the transverse and longitudinal mixing coefficients and how these coefficients are affected by the longitudinal flow nonuniformity. Dedicated field experiments and data analysis are planned to explore the spatial variations of the transverse and longitudinal mixing coefficients.

Data Availability Statement

Data are available here (<http://doi.org/10.5281/zenodo.4748631>)

Acknowledgments

This research was supported by the Commissariat à l'Énergie Atomique et aux Énergies Alternatives (CEA) of Cadarache. The authors would like to express their gratitude to: Alexis Buffet, Mickaël Lagouy, Laura Troudet, Loïc Richard from INRAE Lyon-Grenoble and Sébastien Morilhat from the CEA, for their valuable help and know-how throughout the entire field campaign, which permitted to do an extensive work within a tight schedule.

References

- Abderrezzak, K. E. K., Ata, R., & Zaoui, F. (2015). One-dimensional numerical modelling of solute transport in streams: The role of longitudinal dispersion coefficient. *Journal of Hydrology*, 527, 978–989. <https://doi.org/10.1016/j.jhydrol.2015.05.061>
- Aghababaei, M., Etemad-Shahidi, A., Jabbari, E., & Taghipour, M. (2017). Estimation of transverse mixing coefficient in straight and meandering streams. *Water Resources Management*, 10, 1–19. <https://doi.org/10.1017/s11269-017-1708-4>
- Baek, K. O., Seo, I. W., & Jeong, S. J. (2006). Evaluation of dispersion coefficients in meandering channels from transient tracer tests. *Journal of Hydraulic Engineering*, 132(10), 1021–1032. [https://doi.org/10.1061/\(asce\)0733-9429\(2006\)132:10\(1021\)](https://doi.org/10.1061/(asce)0733-9429(2006)132:10(1021))
- Beltaos, S. (1975). Evaluation of transverse mixing coefficients from slug tests. *Journal of Hydraulic Research*, 13(4), 351–360. <https://doi.org/10.1080/00221687509499693>
- Demetropoulos, A. C., & Stefan, H. G. (1983). Transverse mixing in wide and shallow river: Case study. *Journal of Environmental Engineering*, 109(3), 685–699. [https://doi.org/10.1061/\(asce\)0733-9372\(1983\)109:3\(685\)](https://doi.org/10.1061/(asce)0733-9372(1983)109:3(685))
- Deng, Z.-Q., Singh, V. P., & Bengtsson, L. (2001). Longitudinal dispersion coefficient in straight rivers. *Journal of Hydraulic Engineering*, 127(11), 919–927. [https://doi.org/10.1061/\(asce\)0733-9429\(2001\)127:11\(919\)](https://doi.org/10.1061/(asce)0733-9429(2001)127:11(919))
- Elder, J. W. (1959). The dispersion of marked fluid in turbulent shear flow. *Journal of Fluid Mechanics*, 5, 544–560. <https://doi.org/10.1017/S0022112059000374>
- Fischer, H. B. (1969). The effect of bends on dispersion in streams. *Water Resources Research*, 5(2), 496–506. <https://doi.org/10.1029/WR005i002p00496>
- Fischer, H. B. (1973). Longitudinal dispersion and turbulent mixing in open-channel flow. *Annual Review of Fluid Mechanics*, 5(1), 59–78. <https://doi.org/10.1146/annurev.fl.05.010173.000423>
- Fischer, H. B., & Hanamura, T. (1975). The effect of roughness strips on transverse mixing in hydraulic models. *Water Resources Research*, 11(2), 362–364. <https://doi.org/10.1029/wr011i002p00362>
- Fischer, H. B., List, E. J., Koh, R. C. Y., Imberger, J., & Brooks, N. H. (1979). *Mixing in inland and coastal waters* (pp. 229–278). New York: Academic Press. <https://doi.org/10.1016/b978-0-08-051177-1.50011-8>
- Huai, W., Shi, H., Yang, Z., & Zeng, Y. (2018). Estimating the transverse mixing coefficient in laboratory flumes and natural rivers. *Water, Air & Soil Pollution*, 229(8), 1–17. <https://doi.org/10.1007/s11270-018-3893-z>
- Jeon, T. M., Baek, K. O., & Seo, I. W. (2007). Development of an empirical equation for the transverse dispersion coefficient in natural streams. *Environmental Fluid Mechanics*, 7(4), 317–329. <https://doi.org/10.1007/s10652-007-9027-6>
- Kironoto, B. A., Graf, W. H., & REYNOLDS (1995). Turbulence characteristics in rough uniform open-channel flow. *Proceedings of the Institution of Civil Engineers - Water Maritime and Energy*, 106(4), 333–344. <https://doi.org/10.1680/iwtme.1994.27234>
- Nezu, I., & Nakagawa, H. (1984). Cellular secondary currents in straight conduit. *Journal of Hydraulic Engineering*, 110(2), 173–193. [https://doi.org/10.1061/\(asce\)0733-9429\(1984\)110:2\(173\)](https://doi.org/10.1061/(asce)0733-9429(1984)110:2(173))
- Nezu, I., Tominaga, A., & Nakagawa, H. (1993). Field measurements of secondary currents in straight rivers. *Journal of Hydraulic Engineering*, 119(5), 598–614. [https://doi.org/10.1061/\(asce\)0733-9429\(1993\)119:5\(598\)](https://doi.org/10.1061/(asce)0733-9429(1993)119:5(598))
- Okoye, J. K. (1970). *Characteristics of transverse mixing in open-channel flows*. California Institute of Technology.
- Poncet, N. (2017). Qualification d'un fluorimètre pour l'amélioration de la méthode de jaugeage par dilution globale à la Rhodamine. In *Master internship report*. EDF DTG Grenoble.

- Rutherford, J. C. (1994). *River mixing*. John Wiley & Son Ltd.
- Sayre, W. W., 1979. Shore-attached thermal plumes in rivers. In: In Shen, H. W. (Ed.), (Ed) *Modelling in rivers*.(pp. 15.1–15.44). London. Wiley-Interscience.
- Sayre, W. W., Yeh, T. 1973. *Transverse mixing characteristics of the Missouri River downstream from the cooper nuclear station*, Rep. No.145, University of Iowa.
- Seo, I., Baek, K. O., & Jeon, T. M. (2006). Analysis of transverse mixing in natural streams under slug tests. *Journal of Hydraulic Research*, 44(3), 350–362. <https://doi.org/10.1080/00221686.2006.9521687>
- Seo, I. W., Choi, H. J., Kim, Y. D., & Han, E. J. (2016). Analysis of two-dimensional mixing in natural streams based on transient tracer tests. *Journal of Hydraulic Engineering*, 142(8), 04026020. [https://doi.org/10.1061/\(asce\)hy.1943-7900.0001118](https://doi.org/10.1061/(asce)hy.1943-7900.0001118)
- Smeithlov, B. B. (1990). Effect of channel sinuosity on river turbulent diffusion. *Yangtze River*. (in Chinese), 21(11), 62.
- Song, T., & Chiew, Y. M. (2001). Turbulence measurement in nonuniform open-channel flow using acoustic Doppler velocimeter (ADV). *Journal of Engineering Mechanics*, 127(3), 219–232. [https://doi.org/10.1061/\(asce\)0733-9399\(2001\)127:3\(219\)](https://doi.org/10.1061/(asce)0733-9399(2001)127:3(219))
- Webel, G., & Schatzmann, M. (1984). Transverse mixing in open channel flow. *Journal of Hydraulic Engineering*, 110(4), 423–435. [https://doi.org/10.1061/\(ASCE\)0733-942910.1061/\(asce\)0733-9429\(1984\)110:4\(423\)](https://doi.org/10.1061/(ASCE)0733-942910.1061/(asce)0733-9429(1984)110:4(423))
- Yang, S.-Q., & Chow, A. T. (2008). Turbulence structures in non-uniform flows. *Advances in Water Resources*, 31(10), 1344–1351. <https://doi.org/10.1016/j.advwatres.2008.06.006>
- Yang, S.-Q., Xu, W.-L., & Yu, G.-L. (2006). Velocity distribution in a gradually accelerating free surface flow. *Advances in Water Resources*, 29(12), 1969–1980. <https://doi.org/10.1016/j.advwatres.2006.02.002>
- Yotsukura, N., & Cobb, E. D. (1972). *Transverse diffusion of solutes in natural streams*. US Government Printing Office. <https://doi.org/10.3133/pp582c>
- Yotsukura, N., & Sayre, W. W. (1976). Transverse mixing in natural channels. *Water Resources Research*, 12(4), 695–704. <https://doi.org/10.1029/wr012i004p00695>